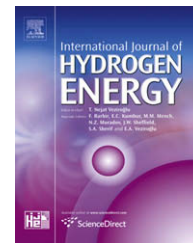


Available at www.sciencedirect.comjournal homepage: www.elsevier.com/locate/he

Steam reforming of hexadecane over a Rh/CeO₂ catalyst in microchannels: Experimental and numerical investigation

J. Thormann^{a,*}, L. Maier^{b,c}, P. Pfeifer^a, U. Kunz^d, O. Deutschmann^{b,c}, K. Schubert^a

^aInstitute for Micro Process Engineering (IMVT), Forschungszentrum Karlsruhe GmbH, Hermann-von-Helmholtz Platz 1, 76344 Eggenstein-Leopoldshafen, Germany

^bInstitute for Chemical Technology and Polymer Chemistry, University of Karlsruhe, Engesserstr. 20, 76131 Karlsruhe, Germany

^cInstitute for Nuclear and Energy Technologies (IKET), Forschungszentrum Karlsruhe GmbH, Hermann-von-Helmholtz Platz 1, 76344 Eggenstein-Leopoldshafen, Germany

^dInstitute of Chemical Process Engineering, Clausthal University of Technology, Leibnizstr. 17, 38678 Clausthal-Zellerfeld, Germany

ARTICLE INFO

Article history:

Received 19 January 2009

Received in revised form

6 April 2009

Accepted 8 April 2009

Available online 14 May 2009

Keywords:

Hexadecane steam reforming

Heterogeneous kinetics

Reaction mechanism

Microchannel reactor

ABSTRACT

Hexadecane is chosen as diesel surrogate to experimentally and numerically investigate diesel reforming in microchannels coated with Rh/CeO₂. A detailed kinetic model is presented and discussed using experimental data on steam reforming of not only hexadecane but also of methane and propane providing a more detailed understanding also of conversion of hexadecane fragments. The turnover frequencies of these linear alkanes were found to be inversely proportional to the number of carbon atoms per hydrocarbon molecule. Based on these results, a kinetic model was developed that links a global reaction equation for the dissociative adsorption of long-chain hydrocarbons with an elementary surface reaction mechanism of steam reforming of methane over Rh/Al₂O₃ catalysts. The model adequately describes the observed correlation between turnover frequency and the number of carbon atoms the hydrocarbon contains. Furthermore, a significant impact of the ceria support on the reformat composition was observed.

© 2009 International Association for Hydrogen Energy. Published by Elsevier Ltd. All rights reserved.

1. Introduction

Today, fuel economy and emission abatement are of great importance in transportation. Fuel cells offer promising routes to both of these challenges; leading however to the questions of hydrogen production and storage. The low energy density of stored hydrogen either in pressurized or liquid form (below 4 kW h/l [1]) limits its widespread use for on-board systems. Although the long-term potential of hydrogen from renewable sources is widely accepted, in the near- to mid-term future hydrogen production will widely rely on fossil fuels. Hence, the production of hydrogen from diesel

fuel is currently of interest as the key benefits of diesel fuel are its existing worldwide infrastructure, a high energy content of around 10 kW h/l [1], easy handling and the prospect biomass-derived and therefore carbon neutral biodiesel or synthetic (GTL) diesel. This prospect could provide a smooth transition from fossil to renewable feedstocks.

For introduction of fuel cells into the transportation market, the hydrogen can be generated on-board and then fed into fuel cells that generate electricity. The use of fuel cell based auxiliary power units (APU) on-board automotive vehicles has the potential to deliver electricity at high efficiencies independently of the engine operation [2]. The

* Corresponding author. Tel.: +49 7247 82 5850; fax: +49 7247 82 3186.

E-mail address: janina.thormann@imvt.fzk.de (J. Thormann).

Nomenclature	
A_k	pre-exponential factor of reaction k , mol, m, s, K
APU	auxiliary power unit
BET	Brunauer–Emmett–Teller
c_i	concentration of species i (in the gas or on the surface), mol/m ³ or mol/m ²
E_{ak}	activation energy of reaction k , J/mol
$F_{cat/geo}$	ratio of catalytic active surface and the geometric surface [-]
GTL	gas to liquid
j_i	diffusive mass flux, mol/s
$j_{i,surf}$	diffusive mass flux at the surface, mol/m ² s
k_{fk}	forward rate coefficient, mol, m, s, K
k_{fk}^{ads}	forward rate coefficient for adsorption reaction, mol, m, s, K
K_s	number of surface reactions [-]
M_i	molar mass of species i , g/mol
N_g	number of gaseous species [-]
N_s	number of surface species [-]
p	pressure, Pa
r	radial coordinate, m
r_{Hex}	reaction rate of hexadecane dissociative adsorption, kmol/m ³ s
R	ideal gas constant, J/mol K
R^2	coefficient of determination [-]
S/C	steam to carbon ratio [-]
S_i^0	sticking coefficient [-]
\dot{s}_i	production rate of species i , mol/m ² s or mol/m ³ s
t	time, s
T	temperature, K
TOF	turnover frequency, mol/mol _{Cat} s
u	axial velocity, m/s
v	radial velocity, m/s
WGS	water-gas shift
X	conversion, %
Y	yield, %
Y_i	mass fraction of species i
z	axial coordinate, m
<i>Greek letters</i>	
β_k	temperature exponent of reaction k
Γ	surface site density, mol/m ²
ε_{ik}	additional model parameter, J/mol
λ	heat conductivity, W/m K
μ	viscosity, Pa s
μ_{ik}	additional model parameter [-]
ν_{ik}	stoichiometric coefficient of converted molecules [-]
ν'_{ik}	stoichiometric coefficient of feed molecules [-]
v_{st}	Stefan velocity, m/s
ω_i	gas-phase reaction rate, kmol/m ³ s
ρ	density, kg/m ³
σ_i	number of surface sites occupied of species i [-]
Θ_i	surface coverage of species i [-]
τ	number of occupied sites [-]
τ_{res}	residence time, s

production of hydrogen from diesel fuel involves a reforming reaction, which produces a hydrogen rich gas and depending on the type of fuel cell, gas cleaning steps to remove CO. Steam reforming produces the highest hydrogen yield in comparison to other reforming technologies. As the steam reforming is an endothermic catalytic reaction, a microstructured reactor is applied to circumvent any heat transfer problems. Microstructure technology achieves high heat and mass transfer rates, good phase contacting, high efficiencies, and compactness and thus, seems to be particularly well suited for the production of hydrogen by fuel reforming [3].

A detailed understanding of the reforming process will support design and optimization of the micro reactors and help to increase their efficiency. Kinetic studies of real diesel fuel are difficult to conduct due to its complex composition. Since hexadecane is its main diesel component, we use hexadecane as surrogate to develop first detailed kinetic models for steam reforming of diesel over rhodium based catalysts [4–8]. Furthermore, the limitations of existing models will be discussed.

The kinetics of methane steam reforming has already been well investigated, a review is given by Rostrup-Nielsen [9]. In contrast to that, only the study from Patel et al. [10] has been published for hexadecane steam reforming. They compared a Power Law model, an Eley–Rideal model, and a Langmuir–Hinshelwood model and estimated the kinetic parameters from experiments in millimeter channels coated with a Rh/Al₂O₃ catalyst. While the Langmuir–Hinshelwood model failed mechanistically, and the Power Law model failed to predict

the results at high S/C ratios, the Eley–Rideal model could reproduce the experimentally measured reaction rates for a wide range of concentrations and temperatures.

Recently, detailed reaction mechanisms for methane partial oxidation [11] as well as methane steam reforming [12–14] were developed, which were able to predict experimental observations reasonably well. In their studies, the software package DETCHEM [15] was used to numerically simulate the catalytic conversion and the reactive flow fields in the reactors.

This paper examines hexadecane reforming in a micro-channel reactor. Previous studies on hydrocarbon reforming by the authors have already been published [16–19]. Based on these results and a previously published surface reaction mechanism for conversion of C1 species adsorbed on Rh/Al₂O₃ [13], an extended reaction mechanism is proposed for modeling the kinetics of hexadecane steam reforming on Rh/CeO₂ assuming dissociative adsorption for hexadecane on Rh.

2. Experimental and data basis

The basis for the numerical model is the reforming experiments already presented in [18,19]. The experimental procedure and equipment are summarized in this section. The experiments were performed in an electrically heated test reactor (Fig. 1) that contained 14 microstructured foils, each with 100 microchannels (width × height × length: 200 μm × 200 μm × 80 mm).

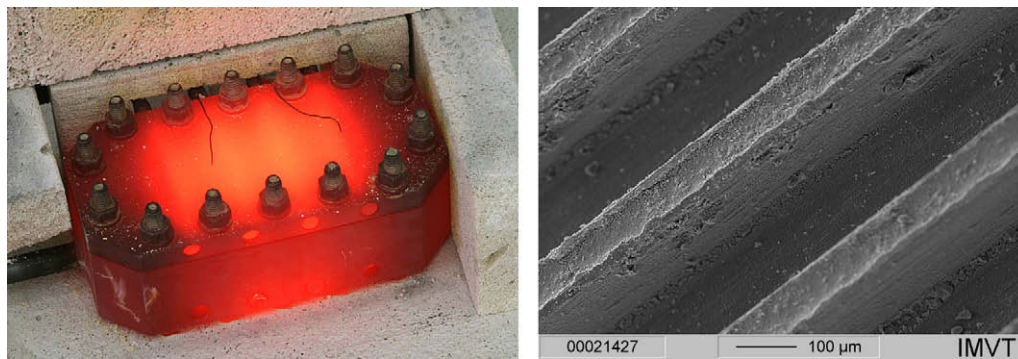


Fig. 1 – Photo of the test reactor (left side) at operation temperature of 973 K and SEM micrograph of microchannels coated with Rh/CeO₂ (right side).

The walls of the microchannels were coated with Rh/CeO₂. An SEM micrograph of the coated channels is shown in Fig. 1 (right). According to microchannel coating experience with several catalyst systems [20], a CeO₂ sol was prepared by mixing 0.7 ml diethanolamine in 30 ml of ethanol, 2.7 g ammonium cerium nitrate, and 1.5 ml concentrated nitric acid for several days and afterwards by diluting with ethanol (1:0.5). This sol was distributed throughout the microchannels, dried at 343 K overnight, and calcinated at 1073 K for 5 h in air. Subsequently, rhodium was deposited on the support layer through the impregnation of the foils with aqueous RhCl₃ solution (0.2 g Rh/l). According to weight measurement of the deposited amount of solution each foil contained 2.8 mg of rhodium and 20 mg of ceria with deviations of 5% and 15%, respectively. Sorption experiments with nitrogen or hydrogen for the calculation of the resulting BET surface area of the foils and the dispersion of rhodium yielded values of 24 m²/g and 4.3% respectively. The catalytic area of the coated foils can also be expressed in terms of $F_{\text{cat}/\text{geo}}$, which is defined by the ratio of the catalytically active surface area to the geometric surface. In our case the calculated factor of $F_{\text{cat}/\text{geo}} = 6.6$ is based on chemisorption measurements determining the amount of catalytically active rhodium molecules. Before each experimental run, the foils were reduced in situ at 1023 K in 2 vol% of hydrogen in nitrogen.

The feed and product streams were analyzed by gas chromatography for hydrocarbons up to C₁₆, permanent gases (hydrogen, nitrogen, oxygen, carbon monoxide and methane), as well as carbon dioxide and water.

Standard conditions have been used for the tests according to the following parameters: an S/C ratio of 4, reactor temperatures between 673 and 973 K and residence times τ_{res} of 75–110 ms.

The first experiments were carried out with methane, propane and hexadecane. The hydrocarbons methane and propane were used to test catalyst activity as well as stability and also to be able to compare their reforming behavior with the long-chain hydrocarbon hexadecane, which was used as a surrogate substance for diesel. These experiments were performed at ambient pressure, 973 K, a steam to carbon ratio of 4 and a space velocity (GHSV) of 48,000 h⁻¹, which corresponds to a residence time τ_{res} inside the microchannels of 75 ms. The turnover frequency (TOF, in moles of hydrocarbons

or C-atoms converted per mole of active rhodium per second) is defined as the velocity of the reaction measured at the catalytic surface. In this study the TOF represents an integral value over the whole reactor instead of the normally applied differential value. For the reforming results (presented in Table 1), maximum errors of 3% for the conversion, 1% for selectivity and yield, and 5% for turnover frequencies have been determined through error propagation. For unbranched alkane fuels, the comparison of the optimum turnover frequency (TOF) in mol_{fuel}/mol_{active Rh s}, which was reached at 973 K, is inversely proportional to the number of C-atoms in the fuel. When considering the conversion of each C atom in the fuel, the TOF values are equal with a mean value of 4.5 ± 0.5 mol_C/mol_{active Rh s}. Wang and Gorte observed that CO_x production rates increased with carbon numbers for the steam reforming of methane, ethane, n-butane and n-hexane over Pd/CeO₂ [21]. Their results presented for the reforming at 700 K also show one TOF value (5.8 mol_C/g_{cat s}) with a deviation of 0.5 mol_C/g_{cat s}). Unfortunately, the authors did not specify whether they consider only the precious metal or also the sum of precious metal and ceria support as catalyst. However, they described that ceria also contributes to the reaction. For this reason no comparison of the TOF values can be made.

For steam reforming of hexadecane on Rh/CeO₂ we use data from our former experimental study [18]. The investigated parameters were: temperature (between 673 K and 973 K), steam to carbon ratio (between S/C values of 3 and 8) reached by adjusting either the steam flow or the fuel flow, and the residence time τ_{res} (between 38 and 220 ms). For

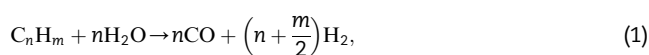
Table 1 – Steam reforming results for methane, propane, and hexadecane on a Rh/CeO₂ catalyst system at standard conditions.

Values at standard conditions	Methane	Propane	Hexadecane
Fuel conversion, X [%]	97.6	100.0	100.0
Hydrogen yield, Y _{H₂} [%]	102.9	97.5	108.0
Selectivity for CO ₂ , S _{CO₂} [%]	44.5	44.9	60.5
Turnover frequency			
TOF [mol _{fuel} /mol _{active Rh s}]	4.1	1.7	0.3
TOF [mol _C /mol _{active Rh s}]	4.1	5.1	4.3

a better understanding of the kinetics of the hexadecane steam reforming reactions, 50 or 100 ml/min of the product gases H₂, CO₂ or CO were added to the feed stream in order to observe the influence of the individual gases on the overall product composition. The parametric study revealed that all parameters influence the selectivities of either CO or CO₂ and thus the water-gas shift reaction. Only a change in the catalyst load (achieved by variation of the residence time or of the fuel flow) or supplemental feeding of hydrogen influences the hexadecane conversion. Hydrogen shows an inhibiting effect but water vapor does not. Water vapor seems to not adsorb on the same active sites as hexadecane and hydrogen.

3. Chemical system

Steam reforming reaction is the reaction of a hydrocarbon with water vapor to form hydrogen and carbon monoxide. It is globally written as:



Due to the water-gas shift reaction (Eq. (2)), the product gas contains also carbon dioxide, which is accompanied by an increase in the produced hydrogen amount. In reality, many side reactions occur on the catalytic surface and they can lead to smaller hydrocarbons, partially oxidated intermediates, and coke formation.

Thermodynamic calculations were carried out with the software HSC Chemistry [22] to determine the thermodynamic equilibrium at given conditions. A comparison with the experimentally derived data is shown in Fig. 2. This comparison reveals that thermodynamic equilibrium (Fig. 2a) and equilibrium conversion (Fig. 2b) are not reached at lower temperatures (673 K up to 823 K), while at higher temperatures than 823 K the experimental results are close to the overall equilibrium composition (equilibrium considerations concerning WGS reaction see later). Beside the components included in Fig. 2a no other substances were detected in the product gas. Methane, which is instable according to the equilibrium calculations, was also not determined in considerable amounts. The theoretical equilibrium composition also contains a considerable amount of C (coke). In the experiments only the product gas was analyzed. Coke formation could only be observed but not quantified when opening the reactor.

4. Modeling of the microchannel

The understanding and optimization of heterogeneous catalyst systems require the knowledge of physical and chemical processes on a molecular level, especially in systems where the interaction of transport and chemistry becomes important. The DETCHEM software package is designed for modeling and simulation of reactive flows including heterogeneous reactions on catalysts and can apply multi-step and

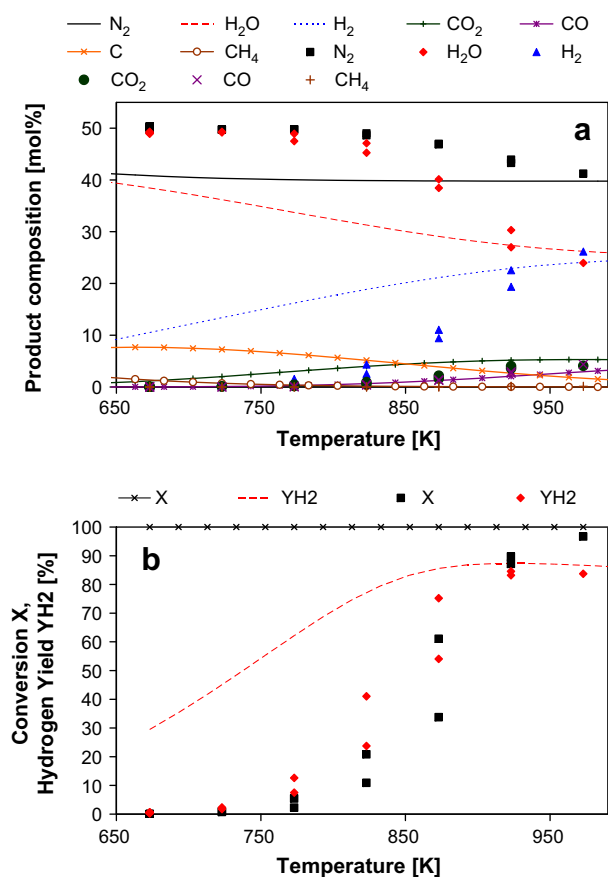


Fig. 2 – Steam reforming of hexadecane: comparison of experimental results (symbols) with thermodynamic (curves) equilibrium calculation results for standard conditions; a) product composition and b) conversion and hydrogen yield versus temperature.

elementary reaction mechanisms on surfaces and in the gas phase [15,23].

The reactor is set-up in a way that all microchannels essentially behave alike as shown in [18]. Hence only a single microchannel needs to be analyzed. The reactive flow field inside the microchannel is laminar and modeled with the steady state, two-dimensional boundary-layer equations using transport coefficients that depend on composition and temperature [24].

Since the experimentally observed temperature difference along the catalytic wall of the microchannels was always below 5 K, isothermal boundary conditions were used in the simulation. The chemical reactions are modeled by detailed reaction schemes for heterogeneous reactions. In this model the mean field approximation is applied for the description of surface reactions [25,26]. The adsorbates on the surface are described in terms of locally varying coverage that represents concentrations of adsorbed molecules randomly distributed on the nanoscale catalyst. The state of the catalytic surface is then described by the temperature T and a set of surface coverages θ_i . Varying surface coverage of adsorbed species is taken into account along the catalytic wall of the microchannel.

4.1. Steady-state flow equations

Although the actual microchannel has a square cross section, it was modeled as an axisymmetric cylinder. Because the spatial gradients perpendicular to the flow direction are small at the conditions applied, an axisymmetric cylinder represents a good approximation of the microchannel.

At given inlet (flow velocity, temperature, pressure, species composition) and boundary conditions (wall temperature of microchannel), the two-dimensional flow field of the fluid is calculated. However, the solution of the Navier–Stokes equations for laminar flow in chemically reacting systems is computationally expensive. Therefore, simpler models such as plug-flow or boundary-layer models are frequently used [24,26]. The boundary-layer approach is used in the DETCHEM^{CHANNEL} code applied in the present work [15,27]. In the boundary layer of a fluid near a surface, convection mainly occurs parallel to the surface. The diffusive transport in the same direction diminishes in comparison to transport perpendicular to the surface. This effect becomes more significant as the gas velocity is increased, for higher Reynolds numbers as long as the flow is laminar. The results achieved by the boundary-layer model can be as accurate as the results from solving the full Navier–Stokes equations at high but laminar flow rates [24]. Mathematically, the character of the equations is simplified from elliptical to parabolic with a time-like coordinate along the channel axis. These requirements result in the following flow field equations:

$$\frac{\partial(r\rho u)}{\partial z} + \frac{\partial(r\rho v)}{\partial r} = 0, \quad (3)$$

$$\frac{\partial(r\rho u Y_i)}{\partial z} + \frac{\partial(r\rho v Y_i)}{\partial r} = -\frac{\partial}{\partial r}(r j_i) + r \omega_i, \quad (4)$$

$$\frac{\partial(r\rho u u)}{\partial z} + \frac{\partial(r\rho v u)}{\partial r} = -r \frac{\partial p}{\partial z} + \frac{\partial}{\partial r} \left(\mu r \frac{\partial u}{\partial r} \right). \quad (5)$$

Here, the following variables are used: z and r – axial and radial coordinates, ρ – density, u and v – axial and radial velocity components, Y_i – mass fraction of species i , j_i – diffusive mass flux of species i , ω_i – gas-phase reaction rate, p – pressure and μ – viscosity. The transport coefficients for radial diffusion μ and the species diffusion fluxes j_i depend on temperature and species composition.

4.2. Surface chemistry model

The surface reaction source terms expressed by diffusion fluxes at the gas–surface interface ($j_{i,\text{surf}}$) are modeled by elementary multi-step reaction mechanism [15,27]. The dynamics of the locally varying surface coverage of adsorbed species i , Θ_i , is determined by

$$\frac{\partial \Theta_i}{\partial t} = \frac{\sigma_i \dot{s}_i}{\Gamma}. \quad (6)$$

Here, σ_i indicates the number of surface sites, that are occupied by species i , \dot{s}_i is the rate of generation or consumption of species i due to adsorption, desorption or chemical reaction, Γ is the surface site density, i.e., the number of adsorption sites per catalytic surface area. The surface site density can be

calculated from the catalyst material. For rhodium a surface site density of $\Gamma = 2.77 \times 10^{-9}$ mol/cm² is used in this model. At steady-state Eq. (6) becomes a set of coupled, non-linear algebraic equations. The net rate of adsorption and desorption of gas-phase species is equal to the diffusive mass flux at the surface, $j_{i,\text{surf}}$, in the radial direction. Convective fluxes vanish in steady state so long as no mass is exsposed or ablated. Hence, the following boundary condition applies for the flux j_i at the inner microchannel wall in Eq. (4):

$$j_{i,\text{surf}} = j_i + \rho Y_i v_{\text{st}} = F_{\text{cat/geo}} \cdot \eta M_i \dot{s}_i, \quad (7)$$

where $j_{i,\text{surf}}$ is the diffusive mass flux at the surface, M_i the molar mass of species i , v_{st} is the Stefan velocity, and $F_{\text{cat/geo}}$ is the ratio between the catalytically active surface area and geometric surface area of microchannel. For the reactor under investigation, this ratio is 6.6 (see Section 3). Since no washcoat is applied in the present study, the effectiveness factor for diffusion within the washcoat, η , is unity. The total molar production rate of species i by surface reactions is given by

$$\dot{s}_i = \sum_{k=1}^{K_s} \nu_{ik} k_{fk} \prod_{j=1}^{N_g+N_s} c_j^{\nu_{jk}}, \quad (8)$$

where K_s is the number of surface reactions (including adsorption and desorption); ν_{ik} (reactants) and ν_{jk} (products) are the stoichiometric coefficients and N_g and N_s are the number of gas-phase and surface species, respectively. The concentrations c_j of adsorbed species are given in mol/m².

The temperature dependence of the rate coefficients is described by a modified Arrhenius expression:

$$k_{fk} = A_k T^{\beta_k} \exp \left[\frac{-E_{ak}}{RT} \right] \prod_{i=1}^{N_s} \Theta_i^{\mu_{ik}} \exp \left[\frac{\varepsilon_{ik} \Theta_i}{RT} \right]. \quad (9)$$

Here A_k represents the pre-exponential factor, β_k the temperature exponent, and E_{ak} the activation energy of reaction k . Coefficients μ_{ik} and ε_{ik} describe the dependency of the rate coefficients on the surface coverage of species i due to possible changes in the energy potential of the surface.

Sticking coefficients are commonly used for adsorption reactions and are converted to conventional rate coefficients according to

$$k_{fk}^{\text{ads}} = \frac{S_i^0}{\Gamma^\tau} \sqrt{\frac{RT}{2\pi M_i}}, \quad (10)$$

with S_i^0 , the sticking coefficient; and τ , the number of sites occupied by adsorbed species.

The computational tool DETCHEM^{CHANNEL} [15,27] is applied to treat the problem numerically. At given inlet conditions, the boundary-layer equations are solved by integration along the axial direction through a method-of-lines procedure. The radial derivatives are discretized by a finite-volume method. The resulting differential-algebraic equation system is integrated using the semi-implicit extrapolation solver LIMEX [28].

5. Heterogeneous reaction mechanism

The mechanism used for modeling reforming of hexadecane consists of 45 reactions with 8 gaseous species and 13

adsorbed species (marked by (s)). The detailed C1-reaction mechanism of this model (see Table 2) is based on an earlier study on the steady-state partial oxidation of methane on Rh/Al₂O₃ [11] that was extended to model steam reforming over Rh/Al₂O₃ [13]. The reversible steps of hydrogen-assisted CO decomposition (reactions (23)–(26), (43), (44) in Table 2) were introduced to improve prediction of methanation and water-gas shift reactions. Kusama et al. [29] suggested CO decomposition as the rate-limiting step in the methanation process. Subsequently, Fisher and Bell [30] and Wang et al. [31] proposed CO hydrogenation via an H_xCO intermediate. Yan et al. [32] observed these intermediate species with time resolved FTIR. Furthermore HCO is proposed to be important in metal – support interaction and oxygen spill-over

reactions on Rh-doped ceria [33]. Simulations performed with this mechanism showed that the steady-state surface coverage distribution at 973 K consists 88% free rhodium sites, 10% CO and 2% other species. Thus, the total surface coverage is low at the conditions investigated; the dependence of the rate coefficients on the surface coverage can be neglected for all adsorbates except for carbon monoxide. The fitting parameter $\varepsilon_{\text{CO}} = 50$ kJ/mol is included in the mechanism to describe the change in activation energy coverage when taking into account the lateral interaction of the adsorbed CO molecules.

In addition to the elementary reactions, a global reaction for the dissociative adsorption of hexadecane on the catalyst surface is set-up:

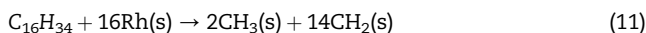
Table 2 – Surface reaction mechanism, from [11].

	Reactions	A [mol, cm, s, K] ^a	S _i ⁰ [-]	E _A [kJ/mol]	ε_{CO} [kJ/mol]
(1)	H ₂ + 2Rh(s) → 2H(s)		0.01	0.0	
(2)	2H(s) → H ₂ + 2Rh(s)	3.0 × 10 ²¹		77.8	
(3)	O ₂ + 2Rh(s) → 2O(s)		0.01	0.0	
(4)	2O(s) → O ₂ + 2Rh(s)	1.33 × 10 ²²		355.2	
(5)	CH ₄ + Rh(s) → CH ₄ (s)		8.0 × 10 ⁻³	0.0	
(6)	CH ₄ (s) → CH ₄ + Rh(s)	2.0 × 10 ¹⁴		25.1	
(7)	H ₂ O + Rh(s) → H ₂ O(s)		0.1	0.0	
(8)	H ₂ O(s) → H ₂ O + Rh(s)	6.0 × 10 ¹³		45.0	
(9)	CO ₂ + Rh(s) → CO ₂ (s)		1.0 × 10 ⁻⁵	0.0	
(10)	CO ₂ (s) → CO ₂ + Rh(s)	3.0 × 10 ⁸		21.7	
(11)	CO + Rh(s) → CO(s)		5.0 × 10 ⁻¹	0.0	
(12)	CO(s) → CO + Rh(s)	1.0 × 10 ¹³		133.4	50.0
(13)	H(s) + O(s) → OH(s) + Rh(s)	5.0 × 10 ²²		83.7	
(14)	OH(s) + Rh(s) → H(s) + O(s)	3.0 × 10 ²⁰		37.7	
(15)	H(s) + OH(s) → H ₂ O(s) + Rh(s)	3.0 × 10 ²⁰		33.5	
(16)	H ₂ O(s) + Rh(s) → H(s) + OH(s)	5.0 × 10 ²²		106.4	
(17)	2OH(s) → H ₂ O(s) + O(s)	3.0 × 10 ²¹		100.8	
(18)	H ₂ O(s) + O(s) → 2OH(s)	3.0 × 10 ²¹		171.8	
(19)	C(s) + O(s) → CO(s) + Rh(s)	5.0 × 10 ²³		97.9	
(20)	CO(s) + Rh(s) → C(s) + O(s)	3.7 × 10 ²¹		169.0	50.0
(21)	CO(s) + O(s) → CO ₂ (s) + Rh(s)	1.0 × 10 ¹⁹		121.6	
(22)	CO ₂ (s) + Rh(s) → CO(s) + O(s)	5.0 × 10 ²¹		115.3	
(23)	CO(s) + H(s) → HCO(s) + Rh(s)	5.0 × 10 ¹⁹		108.9	
(24)	HCO(s) + Rh(s) → CO(s) + H(s)	3.7 × 10 ²¹		0.0	-50.0
(25)	HCO(s) + Rh(s) → CH(s) + O(s)	8.0 × 10 ²³		59.5	
(26)	CH(s) + O(s) → HCO(s) + Rh(s)	3.7 × 10 ²¹		167.5	
(27)	CH ₄ (s) + Rh(s) → CH ₃ (s) + H(s)	5.5 × 10 ²⁰		61.0	
(28)	CH ₃ (s) + H(s) → CH ₄ (s) + Rh(s)	3.7 × 10 ²¹		51.0	
(29)	CH ₃ (s) + Rh(s) → CH ₂ (s) + H(s)	3.7 × 10 ²⁴		103.0	
(30)	CH ₂ (s) + H(s) → CH ₃ (s) + Rh(s)	3.7 × 10 ²¹		44.0	
(31)	CH ₂ (s) + Rh(s) → CH(s) + H(s)	3.7 × 10 ²⁴		100.0	
(32)	CH(s) + H(s) → CH ₂ (s) + Rh(s)	3.7 × 10 ²⁴		68.0	
(33)	CH(s) + Rh(s) → C(s) + H(s)	3.7 × 10 ²¹		21.0	
(34)	C(s) + H(s) → CH(s) + Rh(s)	3.7 × 10 ²¹		172.8	
(35)	CH ₄ (s) + O(s) → CH ₃ (s) + OH(s)	1.7 × 10 ²⁴		80.3	
(36)	CH ₃ (s) + OH(s) → CH ₄ (s) + O(s)	3.7 × 10 ²¹		24.3	
(37)	CH ₃ (s) + O(s) → CH ₂ (s) + OH(s)	3.7 × 10 ²⁴		120.3	
(38)	CH ₂ (s) + OH(s) → CH ₃ (s) + O(s)	3.7 × 10 ²¹		15.1	
(39)	CH ₂ (s) + O(s) → CH(s) + OH(s)	3.7 × 10 ²⁴		114.5	
(40)	CH(s) + OH(s) → CH ₂ (s) + O(s)	3.7 × 10 ²¹		36.8	
(41)	CH(s) + O(s) → C(s) + OH(s)	3.7 × 10 ²¹		30.1	
(42)	C(s) + OH(s) → CH(s) + O(s)	3.7 × 10 ²¹		136.0	
(43)	CO(s) + H(s) → C(s) + OH(s)	3.7 × 10 ²¹		142.8	
(44)	C(s) + OH(s) → CO(s) + H(s)	3.7 × 10 ²⁰		25.5	

a Depending on reaction order.

Table 3 – Kinetic parameters for dissociative adsorption of hexadecane on the rhodium surface (see reaction (11)).

Parameter	A	E_A	β	e_1	e_2
Estimated value	1138 mol m s K	71.0 kJ/mol	0.2	0.495	0.900



This approach is based on experimental observations of the maximum turnover frequencies for hydrocarbons with different carbon lengths, shown in Section 2, Table 1. Regarding the turnover frequencies for the whole fuel molecule (in $\text{mol}_{\text{fuel}}/\text{mol}_{\text{active Rh s}}$), this table reveals that the turnover frequencies decrease from 4.1 $\text{mol}_{\text{fuel}}/\text{mol s}$ for methane down to 0.3 $\text{mol}_{\text{fuel}}/\text{mol s}$ for hexadecane. When the turnover frequencies are calculated for each carbon atom in the hydrocarbon molecule which is converted per active rhodium site and time ($\text{mol}_C/\text{mol}_{\text{active Rh s}}$), then it is obvious that the conversion of each carbon needs the same time and number of active sites; that is to say, the turnover frequencies for methane, propane and hexadecane are all very similar, i.e., 4–5 $\text{mol}_C/\text{mol}_{\text{active Rh s}}$ (deviation of $\pm 22\%$).

For the reaction in equation (10) the following reaction rate equation r along the microchannel results:

$$r_{\text{Hex}} = A \cdot T^\beta \cdot e^{-\frac{E_A}{RT}} \cdot c_{\text{Hex}}^{e_1} \cdot [\Theta_{\text{Rh}(s)} \cdot T_{\text{Rh}}]^{e_2} \quad (12)$$

Initial and boundary conditions of the simulations are taken from the experimental conditions. Hence, the input data for the simulation are feed gas composition, mean gas velocity at the entrance of the reactor, the isothermal reactor temperature, and channel dimensions (length 80 mm and hydraulic diameter 200 μm).

The results of the parameter estimation for the hexadecane adsorption equation (see Eq. (12)) are presented in Table 3.

6. Simulation results and discussion

The product gas compositions calculated are compared with the measured product gas compositions for all 98 performed experiments and are shown in Fig. 3. The coefficient of determination for CO_2 is 0.61. For other components this coefficient reaches at least 0.71. As the coefficient R^2 represents a quadratic rather than linear dependency, the lower coefficient for CO_2 (by only 0.1) exhibits deficiencies in the prediction of the CO_2 formation by the model. A similar trend can be seen when considering the number of experimental values which are adequately predicted by the model. We defined adequately predicted as data points in the parity plots which are within the margins of $\pm 20\%$ deviation. For CO only 9 data points are within these boundaries, followed by CO_2 with only 23. The product gas concentrations of hexadecane, hydrogen and water are better predicted. Both statistical analyses lead to the assumption that the hexadecane conversion is well modeled, whereas all surface reactions

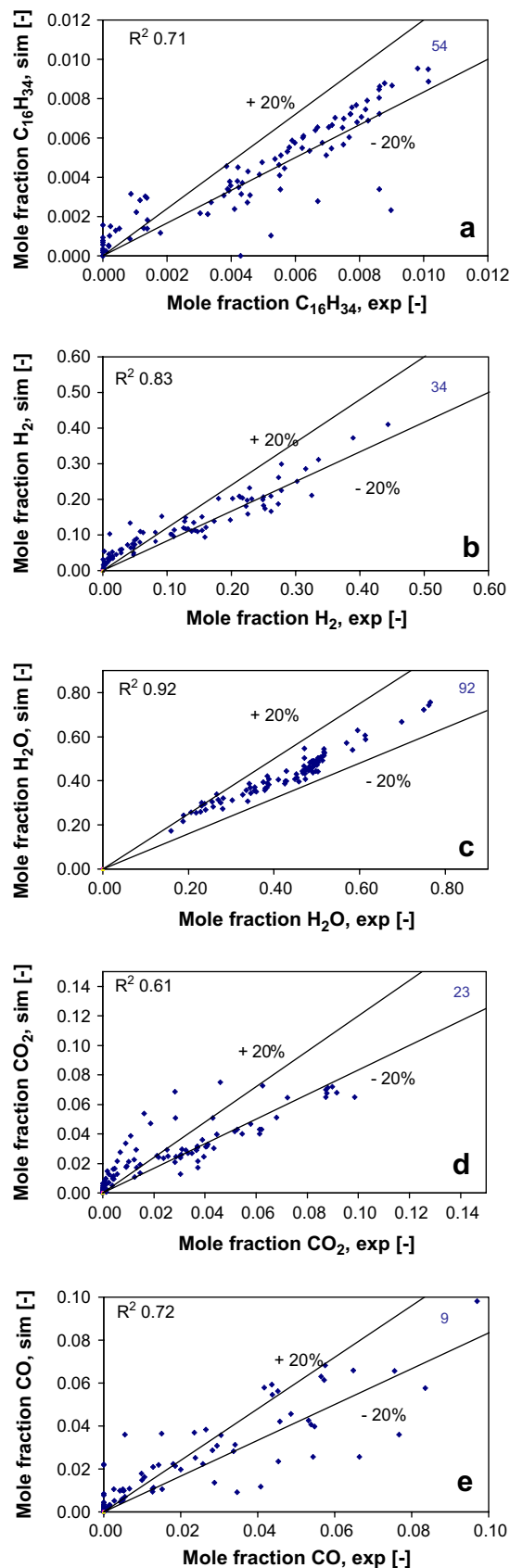


Fig. 3 – Parity plots for hexadecane reforming simulation values compared to experimental data for a) hexadecane, b) H_2 , c) H_2O , d) CO_2 and e) CO at standard conditions.

affecting the equilibrium between CO and CO₂ seem to be inadequately predicted.

Fig. 4 shows the conversion and hydrogen yield for the experiments at the so-called standard conditions (S/C ratio of 4, temperatures between 673 K and 973 K and residence times τ_{res} of 75–110 ms). The maximum deviation for the conversion is 16% and for the hydrogen yield is 32%. The discrepancy in the hydrogen yield between the model and experimental data is greater at temperatures above 873 K.

In Fig. 5 the modeled mass fractions of CO₂ and CO are compared to the experimental data and thermodynamic equilibrium calculations. These thermodynamic equilibrium values were calculated from the experimental output product composition, i.e. hydrogen, carbon monoxide, carbon dioxide and water. Unconverted hexadecane was neglected in these calculations to obtain information on the corresponding water-gas shift equilibrium only. Depending on the position of the experimental values of CO and CO₂ with respect to the equilibrium further information about the mechanism (consecutive or direct CO₂ formation from hexadecane) can be gained. The experimental carbon dioxide product concentration fits well the water-gas shift equilibrium values for the temperatures up to 773 K, but above this temperature the experiments produce less CO₂ than predicted according to the WGS reaction. Vice versa for the carbon monoxide: at higher temperatures is more CO in the reformat than predicted by the WGS equilibrium.

Fig. 5 also explains the deviation between the experimental data and the simulated data for CO and CO₂ (e.g. at 973 K 22% and 25% respectively): the deviation is in the same range as the difference between the measured values and the values at equilibrium (corresponding difference at 973 K is 20% and 18% respectively). Thus, the model underestimates the amount of H₂ (see Fig. 4b) and the CO₂/CO ratio (Fig. 5a) at temperatures above 773 K. For the H₂ concentrations the effect is low, but for the CO₂/CO ratio the deviations are much more visible.

The simulation of the hexadecane conversion can also be used to predict experimental data at different reaction conditions. Earlier studies, described in detail in [18,19], showed that the temperature, variation of the S/C ratio by adjustment of the hexadecane flow, the residence time, and the supplemental feeding of hydrogen have a direct effect on the reforming reaction (1), whereas the variation of the S/C ratio through adjustment of the steam flow or supplemental feeding of CO or CO₂ does not affect the reforming reaction (1). This stands in accordance with the observation of Wei and Iglesia [34] that the reaction rate was dependent on the methane partial pressure and independent of the partial pressure of water or CO₂.

Based on these observations only the parameters affecting the hexadecane conversion are taken into account in the following sections. Fig. 6 depicts the directions of the changes with different parameters are well simulated but that the magnitudes of the changes are smaller than observed. The simulation tends to underestimate influencing effects. This can be seen for example in Fig. 6a for the simulation curve for the lowest S/C ratio, where the jump to higher conversion at 873 K is not well depicted. Another example is the inhibiting effect in Fig. 6c of hydrogen, where at low temperatures the conversion is overestimated when supplemental hydrogen is

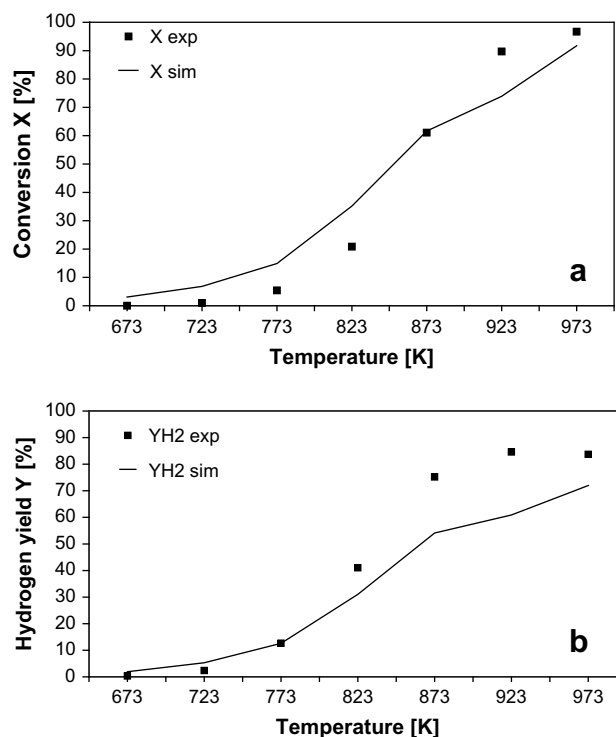


Fig. 4 – Comparison of measured and modeled a) hexadecane conversion and b) hydrogen yield at standard conditions.

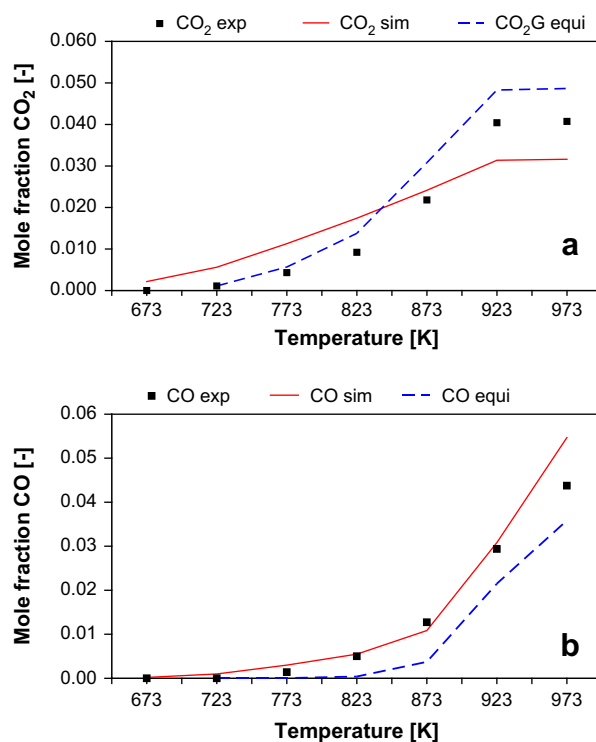


Fig. 5 – Comparison of a) CO₂ and b) CO mole fractions for standard conditions; measured (symbols), modeled (lines), and WGS equilibrium (dashed lines).

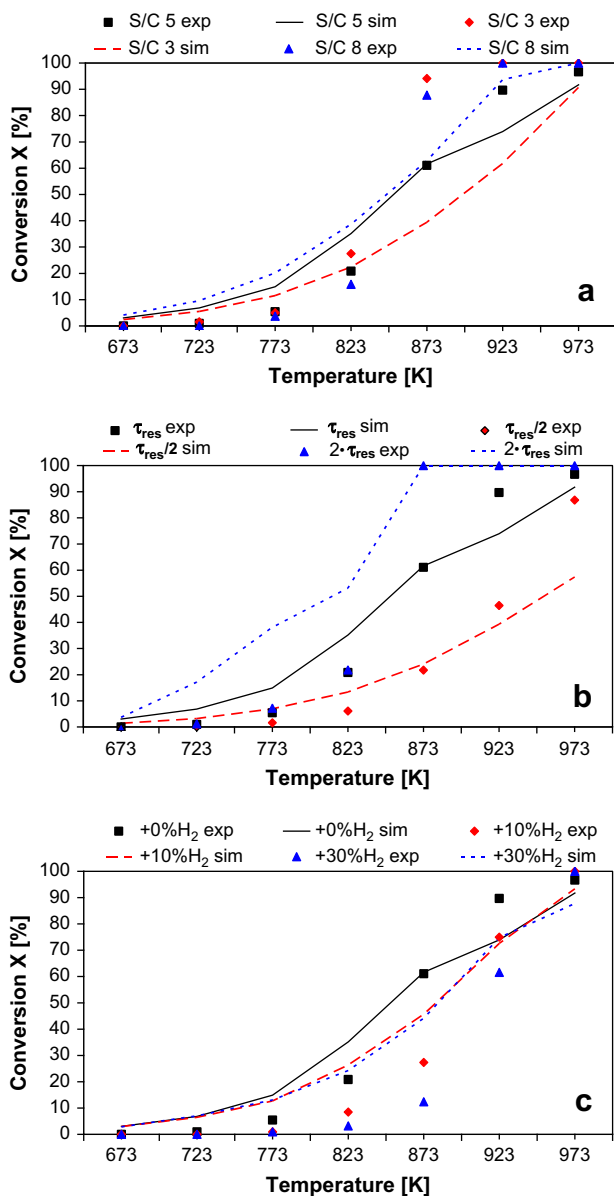


Fig. 6 – Comparison of measured (exp) and modeled (sim) hexadecane conversion at different conditions and temperatures 673–973 K, variation of a) steam to carbon ratio (3, 5, 8); b) residence time (τ_{res} of 75–110 ms, half of the standard residence time $\tau_{res}/2$ and double the standard residence time $2 \times \tau_{res}$); and c) supplemental H₂ feeding (no H₂, supplemental 10% and 30% of H₂).

fed. However, it can be stressed that, overall, the trends of parameter variation are sufficiently well simulated to predict the effects of other reaction conditions.

In addition to the product composition, profiles inside the microchannel can also be computed. The composition and conversion of hexadecane reforming are plotted versus microchannel length in Fig. 7 for standard conditions at 973 K. Due to the decreasing reactant concentration, the rate of reforming decreases along the flow direction.

Fig. 8 shows in more detail the simulated species fractions along the microchannel for the reforming experiment at

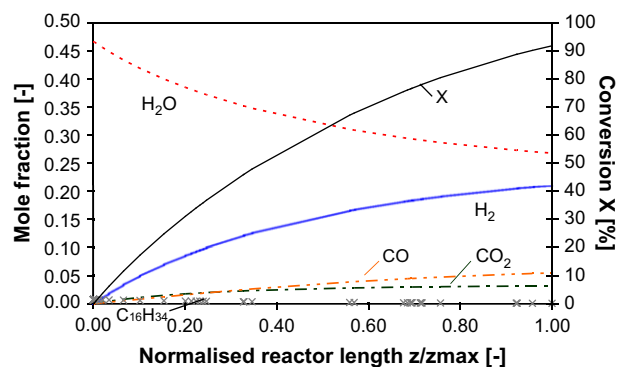


Fig. 7 – Reformate composition (balance is nitrogen) and conversion X of hexadecane reforming along the length of the microchannel at 973 K and standard conditions.

873 K, with a steam to carbon ratio of 8 and a residence time of 85 ms. A maximum in the CO concentration is observed in the middle of the channel length. This is in accordance with the assumption derived from the position of the experimental values of CO and CO₂ in relation to the WGS equilibrium, i.e. that CO is produced from hexadecane and subsequently converted to CO₂. According to Fig. 8 the consecutive shift reaction happens mainly in the second half of the channel length.

6.1. Impact of ceria support

Comparison of simulated and experimental results revealed an adequate description of the hexadecane reforming reaction (Eq. (1)) and its conversion by the applied model. Whereas the water-gas shift equilibrium (Eq. (2)) is not so well depicted by this model. This may be explained by the fact that the detailed surface reaction mechanism used, was developed for pure rhodium catalysts. The extension of surface reaction mechanism account for the impact of ceria support is required for

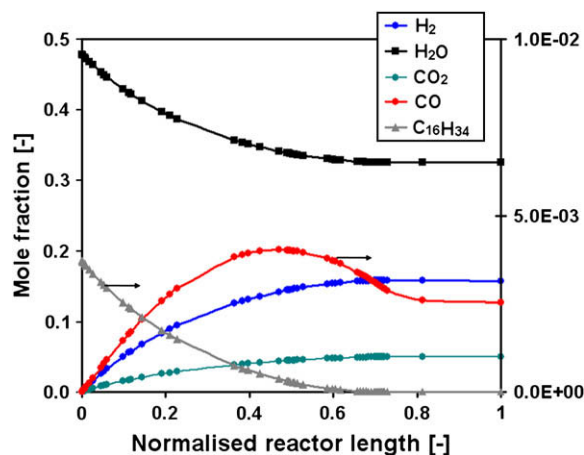


Fig. 8 – Gas composition of hexadecane reforming along the microchannel at 873 K, a steam to carbon ratio of 8, and a residence time τ_{res} of 85 ms.

better description of reforming of higher hydrocarbons on Rh/CeO₂ catalyst.

Ceria-supported precious metals are known to be better catalysts for steam reforming of hydrocarbons, compared to their alumina- or silica-supported counterparts [21,35,36]. Furthermore, the ceria-supported metals simultaneously catalyze the WGS reaction well, even better than either precious metals or ceria alone [33,37]. Platinum, palladium and rhodium supported by ceria show very similar rates for hydrocarbon reforming and the water-gas shift reaction [21,37,38].

There are strong evidences that the support is not inert and the inverse spill-over steps attribute an active role to the support, depending upon its ability to adsorb water and allow surface diffusion of water and oxygen [31,33,39].

The following additional reactions can be proposed to extend the detailed surface reaction mechanism for including the impact of the ceria support. They describe the adsorption and reaction of water on CeO₂ (reactions (13)–(15)) and an inverse spill-over step accompanied by oxygen migration from cerium to the catalyst (reaction (16)):



Here, s₁ indicates the ceria active site and s is the rhodium active site (according to surface chemistry model described in Section 5).

Wang et al. [31] assume that water adsorbs on the support as Brønsted acids and bases. At sufficiently high temperatures but still slow desorption, a mobile intermediate can be formed from the recombination of these acids and bases. This intermediate would be hydrogen bonded to the support and capable of migrating to the Rh surface. The equilibrium (reaction (15)) was suggested at first on Al₂O₃ by Peri [40].

Two different mechanisms for steam reforming of hydrocarbons and water-gas shift reaction are possible to account for the impact of ceria support with additional reactions (13)–(16):

- I. Water is adsorbed on the surface of the ceria support and dissociated into adsorbed hydrogen and oxidized ceria. As hydrogen desorbs from the surface, the atomic oxygen migrates to the precious metal and reacts with the dissociatively on the precious metal surface adsorbed hydrocarbon molecule to form CO. CO is oxidized to CO₂ on the metal surface (Fig. 9 left side).
- II. Oxidation of hydrocarbon to CO accrues on the metal surface as at I, whereas CO₂ is produced via the WGS reaction on the ceria support (Fig. 9 right side). The entire surface reaction follows a Langmuir–Hinshelwood mechanism with species adsorbed at two different sites. The WGS as well as the reforming reaction are controlled by two steps: the transfer of oxygen from ceria to the metal interface and the rate of reoxidation of ceria.

The reaction steps in the overall water-gas shift reaction as oxygen transfer from water to the catalyst and from the catalyst to CO in the mechanism I were suggested by Twigg [41] and Rhodes et al. [42].

The steps proposed in mechanism II for steam reforming of hydrocarbons on precious metal ceria catalyst systems were postulated by Wang and Gorte, Craciun et al. as well as Kurungot and Yamaguchi [21,35,36] and for water-gas shift reaction by Bunluesin et al., Hilaire et al., Sun et al. [37,43,44].

Shido and Iwasawa [33] as well as Jacobs et al. [39] postulate a surface formate mechanism for the WGS reaction over ceria:



Partial reduction of the ceria surface leads to the formation of bridging OH groups and these were found to react with CO to form formate, which then decomposes. Their experiments were performed at quite low temperatures (433–583 K). It may

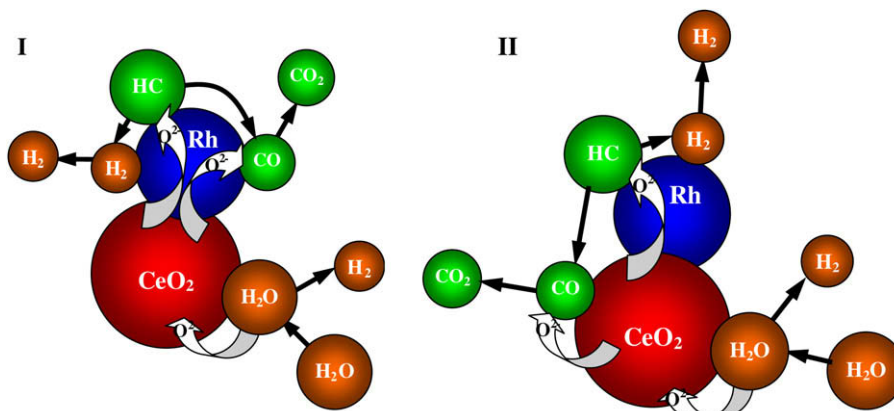


Fig. 9 – Scheme for hydrocarbon steam reforming and water-gas shift reaction on Rh/CeO₂ according to mechanisms I and II.

be assumed that at higher temperature the desorption of CO from the metal and the dissociation of formate on the support are fast and a different mechanism is more likely to occur on the metal [31].

At the moment still additional fundamental studies are required to get the kinetic parameters for reactions (13)–(18) and further kinetic studies for both mechanisms on rhodium/ceria systems.

So Rh/CeO₂ catalysts are known to be good steam reforming and water-gas shift catalysts. The observation of good hexadecane reforming performance but failure to attain the water-gas shift equilibrium especially at high temperatures can result from the high calcination temperature of 1073 K applied during the catalyst preparation. This calcination temperature was chosen to be higher than the high steam reforming temperature of up to 973 K and the even higher catalyst regeneration temperature of 1023 K. Bunluesin et al. [37,45] and Craciun et al. [35,38] revealed that steam reforming as well as water-gas shift reaction rates diminish heavily when the calcination is performed at high temperatures. This activity loss occurs sharply in the 1075–1275 K temperature range due to the loss of ceria support's oxygen transfer property resulting from a change in its structure (larger crystallite sizes). So in this case with the calcination temperature of 1073 K the activity loss for the oxygen transport already starts to appear. Thus, this limited oxygen transfer seems now only able to prevent carbon production and to oxidize the hydrocarbons to CO. Especially at high temperatures with high hydrocarbon conversions, the limited oxygen transfer could not be sufficient anymore to fully oxidize the hydrocarbons to CO₂. One possibility to enhance the WGS activity of Rh/CeO₂ also at high temperatures could be the stabilization of the ceria support with additional zirconia. The mixed oxide maintains its properties at higher calcination temperatures because it appears to prevent the sintering of small ceria clusters [45].

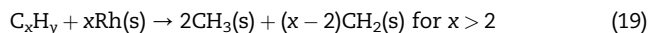
6.2. Simulation of the partial pressure dependence of TOF

The turnover frequency for unbranched alkane fuels is inversely proportional to the reciprocal value of the number of C-atoms per fuel molecule (Section 2). The TOF of each C unit in the fuel is constant at around 4–5 mol_C/mol_{active Rh} s. The approach used in the numerical model for the dissociative adsorption of hexadecane on the catalyst surface in the global reaction equation (Eq. (11), Section 5) is also based on this observation.

In our experiments different molar flow rates and thus partial pressures for methane, propane, and hexadecane were used with the same steam to carbon ratio of 4. Nitrogen flow was used to keep the residence time for each C unit constant. The different partial pressures of the fuels may have an impact on the turnover frequencies according to Rostrup-Nielsen [46]. Therefore, a simulation has been performed from which it is possible to estimate the impact of the partial pressure on the TOF for different molecule sizes.

For standard conditions at 973 K, the same molar flows of methane, propane, and hexadecane with adjusted steam flows were taken. For achieving a constant residence time/gas

velocity balancing nitrogen flows were used. For the global reaction of hexadecane reforming, Eq. (6), which is a special case of the general equation, was applied:



Analogously, the propane reforming was also integrated into the model by use of Eq. (19). For methane reforming Eq. (5) from Table 2 was applied. Based on the simulated product gas composition, the number of converted fuel molecules was estimated. This value and the number of active rhodium sites determined by chemisorption measurements were used for the determination of the turnover frequencies.

In Fig. 10, the turnover frequencies of each C unit in the fuel from these simulations are compared with the experimentally determined TOFs. The predicted mean value of 4.13 mol_C/mol_{active Rh} s differs only 8% from the experimental value and thus confirms that the effect of different partial pressures on the turnover frequencies is negligible.

7. Summary and conclusions

The heterogeneous kinetics of hexadecane reforming in microchannels coated with Rh/CeO₂ was studied by kinetic modeling of experimental data and numerical simulation of the reactor. The experimental data provided reforming performance under different conditions (variation of temperature, steam to carbon ratio, residence time, supplemental feeding of product gases and fuel components). The developed model incorporates channel flow, diffusive transport as well as an elementary-like surface reaction mechanism for C₁ species linked with a global reaction equation for the dissociative adsorption of higher hydrocarbons. The elementary steps have been derived from previous studies on the oxidative conversion of C₁ species over rhodium sites supported on alumina. The global reaction equation assumes hexadecane adsorption and decomposition to C₁ fragments on the Rh/CeO₂ surface. This model appropriately predicts the measured conversion of hexadecane but shows deficiencies for the prediction of carbon oxide selectivity. The dissociative adsorption of hydrocarbons as well as the turnover

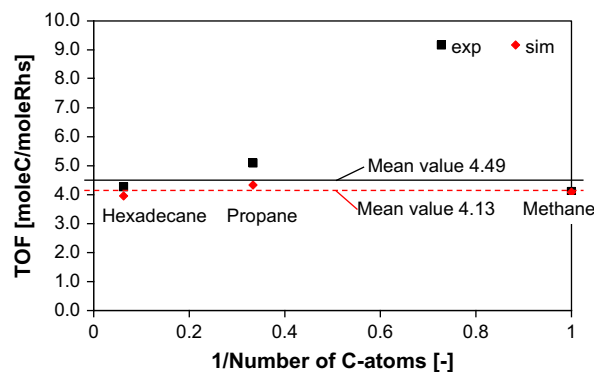


Fig. 10 – Comparison of experimentally determined and simulated turnover frequencies for different fuel molecules.

frequencies (converted fuel molecules per second and active catalyst site) for the reforming of methane, propane, and hexadecane is accurately predicted by the model. Whereas the hydrocarbon conversion seems to take place on the rhodium active sites and is well modeled, the impact of the ceria support and its oxygen transfer properties due to the origin of the elementary steps are not included in the model. This observation calls for the integration of a detailed surface reaction mechanism for CeO₂ into the model.

REFERENCES

- [1] Muradov NZ, Veziroğlu TN. “Green” path from fossil-based to hydrogen economy: an overview of carbon-neutral technologies. *International Journal of Hydrogen Energy* 2008; 33:6804–39.
- [2] Lindström B, Karlsson JAJ, Ekdunge P, De Verdier L, Häggendal B, Dawody J, et al. Diesel fuel reformer for automotive fuel cell applications. *International Journal of Hydrogen Energy* 2009;34:3367–81.
- [3] Dupont N, Germani G, Van Veen AC, Schuurman Y, Schäfer G, Mirodatos C. Specificities of micro-structured reactors for hydrogen production and purification. *International Journal of Hydrogen Energy* 2007;32:1443–9.
- [4] Liu D-J, Kaun TD, Liao HK, Ahmed S. Characterization of kilowatt-scale autothermal reformer for production of hydrogen from heavy hydrocarbons. *International Journal of Hydrogen Energy* 2004;29:1035–46.
- [5] Kopasz JP, Applegate D, Miller L, Liao HK, Ahmed S. Unraveling the maze: understanding of diesel reforming through the use of simplified fuel blends. *International Journal of Hydrogen Energy* 2005;30:1243–50.
- [6] Cheekatamarla PK, Thomson WJ. Catalytic activity of molybdenum carbide for hydrogen generation via diesel reforming. *Journal of Power Sources* 2006;158:477–84.
- [7] Cuttillo A, Specchia S, Antonini M, Saracco G, Specchia V. Diesel fuel processor for PEM fuel cells: two possible alternatives (ATR versus SR). *Journal of Power Sources* 2006; 154:379–85.
- [8] Lutz AE, Bradshaw RW, Bromberg L, Rabinovich A. Thermodynamic analysis of hydrogen production by partial oxidation reforming. *International Journal of Hydrogen Energy* 2004;29:809–16.
- [9] Rostrup-Nielsen JR, Sehested J. Hydrogen and synthesis gas by steam- and CO₂ reforming. *Advances in Catalysis* 2002;47: 65–139.
- [10] Patel D, Gawade P, Goud S, Abraham MA, Lipscomb GG. Steam reforming and combustion kinetics of n-hexadecane for modeling and simulation of a novel catalytic reformer. In: *AIChE annual meeting 2007*, Salt Lake City, 2007.
- [11] Deutschmann O, Schwiedernoch R, Maier L, Chatterjee D. Comparison between calculated and experimentally determined selectivity and conversion for short-contact-time reactors using honeycomb monoliths. In: *Iglesia E, Spivey JJ, Fleisch TH, editors. Natural gas conversion VI. Studies in surface science and catalysis*, vol. 136. Elsevier; 2001. p. 215–58.
- [12] Hecht E, Gupta GK, Zhu H, Dean AM, Kee RJ, Maier L, et al. Methane reforming kinetics within a Ni-YSZ SOFC anode support. *Applied Catalysis A: General* 2005;295:40–51.
- [13] Baumann F, Deutschmann O, Duisberg M, Maier L, Schmidt LD, Sextl G, et al. ATR catalyst for natural gas conversion to hydrogen: performance, modeling, and simulation. In: *13th International congress on catalysis*, Paris, 2004.
- [14] Schädel BT, Deutschmann O. Steam reforming of natural gas on noble-metal based catalysts: predictive modeling. In: *Schmal M, Noronha FB, Sousa-Aguiar EF, editors. Natural gas conversion VIII. Studies in surface science and catalysis*, vol. 167. Elsevier; 2007. p. 207–12.
- [15] Deutschmann O, Tischer S, Kleditzsch S, Janardhanan VM, Correa C, Chatterjee D, et al. DETCHEM software package. version 2.1, www.detchem.com; 2007. Karlsruhe.
- [16] Pfeifer P, Haas-Santo K, Görke O, Thormann J, Schubert K. Small efficient microchannel systems for mobile and decentralised hydrogen production. In: *Geo-Siberia: 2nd international specialized exhibition and scientific congress on geodesy, mapping, geology, geophysics cadaster*, Novosibirsk, Russia, 2006. *Proceedings*; 4. p. 292–301.
- [17] Thormann J, Pfeifer P, Schubert K, Kunz U. Reforming of diesel fuel in a micro reactor for APU systems. *Chemical Engineering Journal* 2008;135:S74–81.
- [18] Thormann J, Pfeifer P, Kunz U, Schubert K. Reforming of diesel fuel in a micro reactor. *International Journal of Chemical Reactor Engineering* 2008;6:P1.
- [19] Thormann J, Pfeifer P, Kunz U, Schubert K. Microstructured reactors for catalytic reforming of higher hydrocarbons. In: *AIChE 2007 annual meeting*, Salt Lake City, 2007. *Proceedings*. p. 246.
- [20] Haas-Santo K, Fichtner M, Schubert K. Preparation of microstructure compatible porous supports by sol-gel synthesis for catalyst coatings. *Applied Catalysis A: General* 2001;220:79–92.
- [21] Wang X, Gorte RJ. A study of steam reforming of hydrocarbon fuels on Pd/ceria. *Applied Catalysis A: General* 2002;224: 209–18.
- [22] Roine A. *HSC chemistry for Windows 5.11*. Outokumpu Research Oy; 2003.
- [23] Minh HD, Bock HG, Tischer S, Deutschmann O. Optimization of two-dimensional flows with homogeneous and heterogeneously catalyzed gas-phase reactions. *AIChE Journal* 2008;54:2432–40.
- [24] Raja LL, Kee RJ, Deutschmann O, Warnatz J, Schmidt LD. A critical evaluation of Navier–Stokes, boundary-layer, and plug-flow models of the flow and chemistry in a catalytic-combustion monolith. *Catalysis Today* 2000;59:47–60.
- [25] Coltrin ME, Kee RJ, Rupley FM. Surface Chemkin: a generalized formalism and interface for analyzing heterogeneous chemical kinetics at a gas–surface interface. *International Journal of Chemical Kinetics* 1991;23:1111–28.
- [26] Deutschmann O. In: *Ertl G, Knözinger H, Schüth F, Weitkamp J, editors. Handbook of heterogeneous catalysis*. 2nd ed. Weinheim: Wiley-VCH; 2007 [chapter 6.6].
- [27] Tischer S, Correa C, Deutschmann O. Transient three-dimensional simulations of a catalytic combustion monolith using detailed models for heterogeneous and homogeneous reactions and transport phenomena. *Catalysis Today* 2001; 69:57–62.
- [28] Deuffhard P, Hairer E, Zangl E. One-step and extrapolation methods for differential-algebraic systems. *Numerische Mathematik* 1987;51:501–16.
- [29] Kusama H, Bando KK, Okabe K, Arakawa H. Effect of metal loading on CO₂ hydrogenation reactivity over Rh/SiO₂ catalysts. *Applied Catalysis A: General* 2000;197:255–68.
- [30] Fisher IA, Bell AT. A comparative study of CO and CO₂ hydrogenation over Rh/SiO₂. *Journal of Catalysis* 1996;162:54–65.
- [31] Wang D, Dewaele O, De Groote AM, Froment G. Reaction mechanism and role of the support in the partial oxidation of methane on Rh/Al₂O₃. *Journal of Catalysis* 1996;159:418–26.
- [32] Yan Q, Wu T, Yang L, Luo C, Weng W, Chao Z, et al. Mechanism study of methane partial oxidation to synthesis gas over a SiO₂-supported rhodium catalyst. *Journal of Natural Gas Chemistry* 2000;9(1):1–7.

- [33] Shido T, Iwasawa Y. Reactant-promoted reaction mechanism for water-gas-shift reaction on Rh-doped CeO₂. *Journal of Catalysis* 1993;141:71–81.
- [34] Wei J, Iglesia E. Structural requirements and reaction pathways in methane activation and chemical conversion catalyzed by rhodium. *Journal of Catalysis* 2004;225:116–27.
- [35] Craciun R, Daniell W, Knözinger H. The effect of CeO₂ structure on the activity of supported Pd catalysts used for methane steam reforming. *Applied Catalysis A: General* 2002;230:153–68.
- [36] Kurungot S, Yamaguchi T. Stability improvement of Rh/ γ -Al₂O₃ catalyst layer by ceria doping for steam reforming in an integrated catalytic membrane reactor system. *Catalysis Letters* 2004;92:181–7.
- [37] Bunluesin T, Gorte RJ, Graham GW. Studies of water-gas-shift reaction on ceria-supported Pt, Pd, and Rh: implications for oxygen-storage properties. *Applied Catalysis B: Environmental* 1998;15:107–14.
- [38] Craciun R, Shereck B, Gorte RJ. Kinetic studies of methane steam reforming on ceria-supported Pd. *Catalysis Letters* 1998;51:149–53.
- [39] Jacobs G, Patterson PM, Graham UM, Crawford AC, Davis BH. Low temperature water gas shift: the link between the catalysis of WGS and formic acid decomposition over Pt/ceria. *International Journal of Hydrogen Energy* 2005;30:1265–76.
- [40] Peri JB. Infrared and gravimetric study of the surface hydration of γ -alumina. *Journal of Physical Chemistry* 1965;69:211–9.
- [41] Twigg MV, editor. *Catalyst handbook*. 2nd ed. Manson Publishing Ltd.; 1996.
- [42] Rhodes C, Hutchings GJ, Ward AM. Water-gas shift reaction: finding the mechanistic boundary. *Catalysis Today* 1995;23:43–58.
- [43] Hilaire S, Wang X, Luo T, Gorte RJ, Wagner J. A comparative study of water-gas-shift reaction over ceria supported metallic catalysts. *Applied Catalysis A: General* 2001;215:271–8.
- [44] Sun J, Desjardins J, Buglass J, Liu K. Noble metal water gas shift catalysis: kinetic study and reactor design. *International Journal of Hydrogen Energy* 2005;30:1259–64.
- [45] Bunluesin T, Gorte RJ, Graham GW. CO oxidation for the characterization of reducibility in oxygen storage components of three-way automotive catalysts. *Applied Catalysis B: Environmental* 1997;14:105–15.
- [46] Rostrup-Nielsen JR. Activity of nickel catalyst for steam reforming of hydrocarbons. *Journal of Catalysis* 1973;31:173–99.